Microchimica Acta (2019) 186: 624
https://doi.org/10.1007/s00604-019-3735-8

ORIGINAL PAPER

Amperometric determination of nitrite by using a nanocomposite prepared from gold nanoparticles, reduced graphene oxide and multi-walled carbon nanotubes

Hao Yu[1,2] · Rui Li[1] · Kai-li Song[1]

Received: 17 February 2019 / Accepted: 2 August 2019 / Published online: 14 August 2019

Abstract

A nanocomposite consisting of gold nanoparticles (AuNP), reduced graphene oxide (rGO) and multi-walled carbon nanotubes (MWCNTs) was synthesized using a co-reduction strategy in ethylene glycol using sodium citrate as the reducing agent. The nanocomposite was successfully characterized using X-ray powder diffraction, scanning electron microscopy and electrochemical methods. The material was deposited on a glassy carbon electrode and then was found to have high electrocatalytic capability for the electrode process of nitrite. This is attributed to the synergic actions of rGO, MWCNTs and AuNPs. Based on this, an amperometric nitrite sensing scheme was worked out that had attractive features: (a) a wide linear range that extends from 50 nM to 2.2 mM, (b) a working potential of 0.80 V (vs.SCE) at pH 5.0, (c) a 14 nM detection limit (at an SNR of 3), and (d) an electrochemical sensitivity of 1201 $\mu A \cdot mM^{-1} \cdot cm^{-2}$. The sensor was successfully applied to the determination of nitrite in the local river water.

Keywords Metal nanoparticles · Carbon materials · Nanocomposite · Chemical co-reduction · Ethylene glycol · Electrochemical sensor · Electrocatalysis · Environmental detection · Water quality analysis · Nitrite

Introduction

There is a variety of methods that can be used for the quantitative detection of nitrite in various samples. Among them, electrochemical techniques have received particular attention due to their outstanding characteristics including high sensitivity, considerable selectivity and simplicity [1]. In order to improve the analytical performance of the electrochemical methods, some nano materials, such as nobel metal, including AuNP [2, 3], PtNP [4], PdNP [5], transition metal oxide [6, 7], as well as carbon-based materials [8, 9] have been synthesized and applied for the determination of nitrite in various samples. In these materials, AuNP have been widely introduced on the electrochemical sensing interface through various ways to enhance the analytical performance of nitrite [10–14]. However, to further improve the electrochemical activity of AuNP to nitrite, it is necessary to control the particle size and the uniformity of its on the electrode surface. For this reason, some carriers are used to load AuNP. It is well known, graphene (GR) has the characteristics of large specific surface area, high conductivity, good chemical stability, and is widely used as a carrier for loading metal nanoparticles. So far, many efforts have been made to prepare AuNP–GR composite to enhance the electrochemical catalytic activity of it to nitrite [15–22]. Nevertheless, there is a strong interaction between the GR sheets, so that most of AuNP in the composite are embedded in its sheets. Hence, they are not available to reactants and their catalytic activity is not be fully utilized. This will compromise its electrochemical sensing capability. Recent researches show that this problem can be partially solved by introducing carbon nanotubes (CNTs) between GR nanosheets [23, 24]. Compared with GR, the GR-CNTs composite also has larger specific surface area and can provide more active sites for loading MNP [25]. For example, some types

Electronic supplementary material The online version of this article (https://doi.org/10.1007/s00604-019-3735-8) contains supplementary material, which is available to authorized users.

✉ Hao Yu
yananyh2013@163.com

[1] College of Chemistry and Chemical Engineering, Yan'an University, Yan'an, China

[2] Shaanxi Key Laboratory of Chemical Reaction Engineering, Yan'an University, Yan'an, China

of AuNP-rGO-CNTs composite materials have been prepared with various methods and used in electrochemical sensing application [26–30].

In this work, the AuNP-rGO-MWCNTs nanocomposite is synthesized using a simple one-step chemical co-reduction strategy. Subsequently, a new electrochemical sensing platform for nitrite based on this nanocomposite was successfully prepared by immobilization of it on a GCE. Under the synergistic action of each component in composite, this sensor has the characteristics of low detection limit, wide dynamic range, high sensitivity and good stability for nitrite. This sensor has also been used to analysis the concentration of nitrite in local river water with satisfactory results.

Experimental

Reagents

Graphene oxide (> 99.9 wt%) were provided by Hengqiu Graphene Technology Co. Ltd. (Suzhou, China, http://graphenechina.en.forbuyers.com) and was used without further purification. Multi-walled carbon nanotubes (MWCNTs, the carbon content was greater than 95%) were purchased from Shenzhen Nanotech Port Co. Ltd. (Shenzhen, China, http://cnanotube.en.ec21.com). Sodium nitrite ($NaNO_2$, A.R.), Ethylene glycol (EG, A.R.), sodium citrate (A.R.), and tetrachloroauric acid tetrahydrate ($HAuCl_4{\cdot}4H_2O$, A.R.) were provided by Shaanxi Pharmaceutical Group Chemical Reagent Co., Ltd. (Xi'an, China, http://www.11467.com/xian/co/124476.htm). All the other reagents used in the experiments were of analytical grade and were not further purified prior to use. All aqueous solutions were prepared in double distilled water with a resistivity greater than 18.3 MΩ.

Apparatus

A CHI660d electrochemical workstation (Shanghai Chenhua Instrument Co., Ltd., Shanghai, China, http://www.chinstruments.com) was used for all the electrochemical experiments. The three-electrode test system was made of the modified electrode as a working electrode, a platinum column electrode as an auxiliary electrode, and a saturated calomel electrode (SCE) as a reference electrode. All the electrode potential values in this work were reference with the SCE. All electrochemical tests were carried out at room temperature. A Quanta 600 scanning electron microscope (FEI/Philips, U.S.A, https://www.fei.com/products/sem/quanta-sem/) was used to record the scanning electron microscopy (SEM) photos at a voltage of 3.0 kV. The test samples were dropped onto the glassy carbon electrode (GCE). A D/Max-2500 X-ray diffractometer (Rigaku/Japan, https://www.rigaku.com/ja) was applied to record to X-ray powder diffraction (XRD) patterns using Cu K_α radiation (λ = 0.15418 nm) in the 2θ range of 5–80°.

Preparation of AuNP-rGO-MWCNTs composite modified electrode

Treatment of MWCNTs: Firstly, 1.0 g of pristine MWCNTs were dispersed in 100 mL nitric acid solution(20%, *v*/v)for 12 h to eliminate the metal impurities. Then the above MWCNTs were dispersed into concentrated nitric acid and sulfuric acid hybrid solution (1:3, v/v) under ultrasonic agitation until a black jelly was obtained. Then, the reaction solution is diluted, filtered and washed with water to remove the residual acid. Finally, the product was dried overnight in vacuum at 60 °C prior to use.

The AuNP-rGO-MWCNTs composite was synthesized according to the literature reported previous with some modification [25]. Firstly, 12.5 mg GO, 37.5 mg MWCNTs and 150 mg sodium citrate were added to 20 mL EG in sequence. After each reagent was added, the solution should be dispersed evenly by ultrasonic dispersion. Then, the mixed solution was dispersed by ultrasound for another 2 h. After that, 6.7 mL EG solution containing 0.1065 g $HAuCl_4{\cdot}4H_2O$ was added to the solution and dispersed for 30 mins. When pH was adjusted to 10.0 with KOH-EG, the hybrid solution was reflux at 120 °C for 6 h. Subsequently, the product was filtered by 0.45 μm filter membrane and washed with double distilled water until the filtrate was free of Cl^-. The product was dried in vacuum for 12 h at 60 °C. Lastly, a dispersion containing 0.5 mg·mL^{-1} of the AuNP-rGO-MWCNTs composite was prepared by ultrasonic dispersion. For comparison, rGO, MWCNTs, and rGO-MWCNTs were also prepared by similar methods.

In this work, the modified electrodes of the above materials were prepared by dropping method. Firstly, the glassy carbon electrode (GCE) was pretreated according to the method reported in literature [14]. Subsequently, 10 μL dispersion solutions of the above AuNP-rGO-MWCNTs, rGO-MWCNTs, rGO, and MWCNTs materials were dropped on GCE. Lastly, these modified electrodes were dried at room temperature and described as AuNP-rGO-MWCNTs/GCE, rGO-MWCNTs/GCE, MWCNTs/GCE, and rGO/GCE, respectively.

Electrochemical measurements

The electrochemical characteristic of this AuNP-rGO-MWCNTs/GCE was investigated using cyclic voltammetry (CV) and electrochemical impedance spectroscopy (EIS) using $[Fe(CN)_6]^{4-/3-}$ couple as a probe. The CV graph was recorded in the potential range of −0.2 − 0.7 V in 0.10 mol·L^{-1} KCl containing 10 mM $K_3Fe(CN)_6$ with the potential scan

rate of 50 mV·s^{-1}. The EIS plots were recorded in a voltage frequency range of 0.01 Hz to 100 KHz with the amplitude of 5 mV. Amperometric detection was performed at 0.8 V in 0.10 mol·L^{-1} phosphate buffer (pH 5.0) with the addition of a certain amount of nitrite. Scheme 1 illustrated the fabrication process of the AuNP-rGO-MWCNTs/GCE and its detection principle for nitrite.

Results and discussion

Preparation and characterization of the AuNP-rGO-MWCNT composite

The XRD patterns of different materials of GO (a), rGO (b), MWCNTs (c), rGO-MWCNTs (d) and AuNP-rGO-MWCNTs (e) are showed in Fig. 1. As shown in this figure, GO gives a board diffraction peak of the (002) plane at 11.35°. However, on the diffraction pattern of rGO (curve b), two new diffraction peaks are given at 25.03 and 43.02°, and the peak of GO at 11.35° disappears. This indicates that GO can be reduced to rGO and the sp^2 hybrid graphene network has been established under the present condition [22, 27–29]. The peak at 25.51° on curve c can be assigned to (002) plane of MWCNTs (curve c). For rGO-MWCNTs composite, two diffraction peaks at 25.86° and 43.12° are observed, which indicate that GO can also be reduced to rGO in this composite (curve d) [22, 27–29]. As expected, there are four peaks located at 38.42°, 44.61°, 64.72° and 77.61° on the pattern of AuNP-rGO-MWCNTs composite (curve e). According to the literature, they are the characteristic diffraction peaks of (111), (200), (220) and (311) planes of cubicstructured Au [18, 28]. This demonstrates that $HAuCl_4$ can be reduced to AuNP in this process. Also, a weak broad

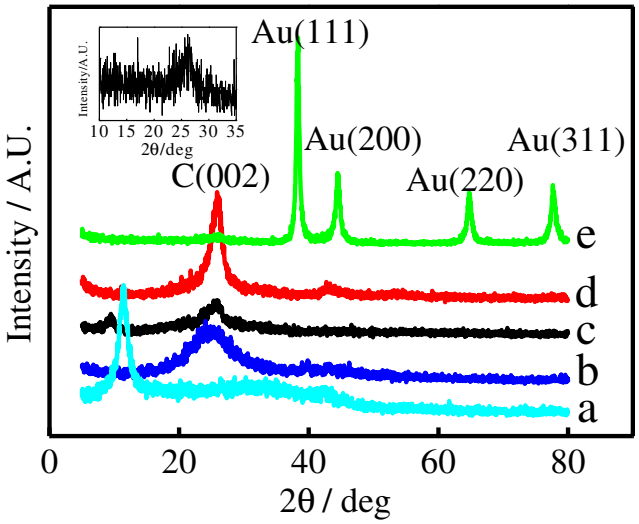

Fig. 1 XRD patterns of various materials. **a** GO, **b** rGO, **c** MWCNTs, **d** rGO-MWCNTs, and **e** AuNP-rGO-MWCNTs

peak of rGO is observed at 25.86°, indicating that GO can be simultaneously reduced to rGO in this composite (insert graph of this figure) [22, 27–29]. The results of the XRD experiment show that the AuNP-rGO-MWCNTs composite material can be obtained by this co-reduction strategy.

Figure 2 gives the typical SEM graphs of various materials modified electrodes. As shown in this figure, the MWCNTs treated with this method has complete structure, and its dispersion uniformity has been obviously improved (Fig. 2a). However, there is a serious accumulation between the graphene layers in rGO (Fig. 2b). This is due to the elimination of oxygen-containing groups in GO during the reduction process, which leads to the restacking of rGO sheets under π-π interaction [31]. In rGO-MWCNTs, MWCNTs are obviously inserted between the rGO layers, and a thinner layer is obtained (Fig. 2c).

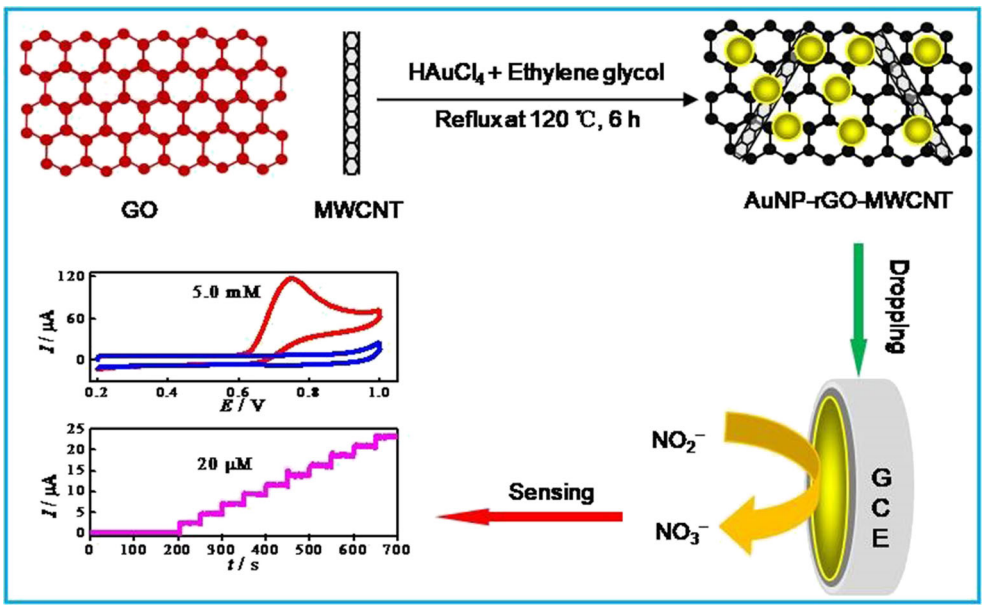

Scheme 1 Illustration of the fabrication process of the AuNP-rGO-MWCNTs/GCE and the sensing principle of this modified electrode for nitrite

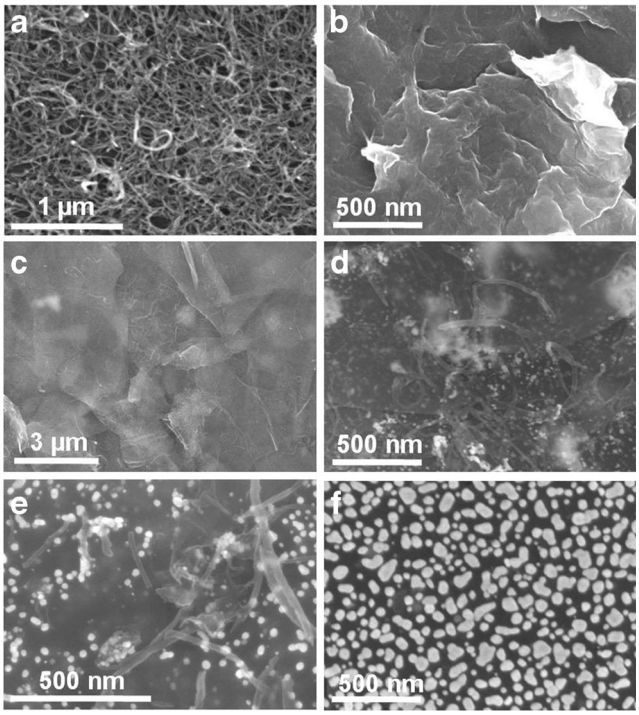

Fig. 2 SEM graphs of different modified electrode of MWCNTs/GCE (**a**), rGO/GCE (**b**), rGO-MWCNTs/GCE (**c**), AuNP-rGO-MWCNTs/GCE (**d** and **e**) and AuNP/GCE (**f**, prepared by electrodeposition)

This demonstrates that the incorporation of carbon nanotubes can reduce the agglomeration of graphene sheets, which is beneficial to obtaining a thinner sheet and increasing the specific surface area of the materials [23, 24]. The SEM graph of AuNP-rGO-MWCNTs/GCE is shown by Fig. 2d, e. It is clearly seen that, firstly, AuNP is mainly loaded on the surface of rGO sheets. The average particle size of AuNP is about 25 nm and has good dispersion (Fig. 2f). Meanwhile, MWCNTs is also inserted into the rGO layers and further improve the dispersion of rGO. Compared with rGO-MWCNTs, the rGO sheet in AuNP-rGO-MWCNTs is thinner, which indicates the introduction of AuNP can also reduce the agglomeration of rGO sheets. These results show that the introduction of MWCNTs and AuNP can obviously improve the dispersion of rGO, and therefore, higher electrochemical activity can be obtained.

Electrochemical characteristic of the AuNP-rGO-MWCNTs/GCE

Electrochemical impedance spectroscopy (EIS) technique can directly explain the changes of interfacial properties of chemical modified electrodes in the modification process [25]. The Nyquist plots of the bare GCE (a), rGO/GCE (b), MWCNTs/GCE (c), rGO-MWCNTs/GCE (d) and AuNP-rGO-MWCNTs/GCE (e) in 0.10 mol·L^{-1} KCl containing 10.0 mM $[Fe(CN)_6]^{4-/3-}$ are shown in fig. S1-A (ESM). It can be seen that the interface charge transfer resistance (R_{et}, the diameter of semicircle on Nyquist plot at high frequency range) of the bare electrode is about 466.7 Ω (a). When rGO is modified on the electrode surface, the R_{et} value decreased to 303.4 Ω (b). It is shown that rGO can enhance the electrochemical activity of the electrode interface. On the other hand, when the electrode is modified with MWCNTs, the R_{et} value also decreases to 180.6 Ω, (curve c). By contrast, it can be seen that MWCNTs have faster charge transfer rate than rGO. This is because of that, on the one hand, the dispersion of rGO is not good and the active area of electrode is small without the action of AuNP and MWCNTs. On the other hand, the residual oxygen-containing groups in rGO also exhibits a certain electrostatic repulsive effect to $[Fe(CN)_6]^{4-/3-}$. For rGO-MWCNTs/GCE, the R_{et} is further reduced to 100.20 Ω (curve c). This indicates that rGO-MWCNTs has faster charge transfer rate than that of any single component. This is because of that MWCNTs can reduce the agglomeration of rGO sheets, and rGO can improve the consecutiveness of MWCNTs. Under the synergistic action of rGO and MWCNTs, the rGO-MWCNTs composite has a larger effective area [23, 24]. As expected, after modifying with AuNP-rGO-MWCNTs, the R_{et} value is further reduced (curve e). This shows that the introduction of AuNP in composite can further accelerate the interfacial charge transfer rate. Accordingly, the CV characteristics of the above electrodes in 0.10 mol·L^{-1} KCl containing 5.0 mM $K_3[Fe(CN)_6]$ are shown in fig. S1-B (ESM). As it can be seen, similar results have been obtained by CV. In conclusion, the addition of MWCNTs in composite can availably reduce the agglomeration of rGO sheet. This makes rGO-MWCNTs composite have a larger specific area and can be used as a promising carrier to load AuNP with high electrochemical activity.

Electrochemical characteristics of nitrite on the AuNP-rGO-MWCNTs/GCE

Figure 3 shows the CV graphs of various electrodes in 0.10 mol·L^{-1} phosphate buffer (pH 5.0) with the addition of various concentration of nitrite (0.0–3.0 mM). As shown in this figure, a little irreversible oxidation peak of nitrite at 0.783 V on bare GCE has been observed (Fig. 3a). There is a linear relationship between the peak current and the concentration of nitrite. The linear regression equation on bare GCE is I_p (μA) = 0.004 + 14.12 $c_{nitrite}$ (mM) (Fig. S2, curve a, ESM). When GCE is modified with AuNP (Fig. 3b), rGO (Fig. 3c) and MWCNTs (Fig. 3d), the current response increases accordingly, indicating that these three materials have electrocatalytic activity for nitrite. The slope of the linear relationship on AuNP/GCE, rGO/GCE and MWCNTs/GCE is 18.21, 17.96, and 18.72 μA·mM^{-1}, respectively (Fig. S2, curve b, c, and d, ESM). However, when GCE is modified with rGO-MWCNTs composite, the slope of the linear relationship of nitrite increases to 21.39 μA·mM^{-1} (Fig. S2, curve e, ESM), and the peak potential of nitrite decreased obviously. This demonstrates that rGO-MWCNTs composite has higher electrochemical activity than the single component. However, on the AuNP-rGO-MWCNTs/GCE, the potential of

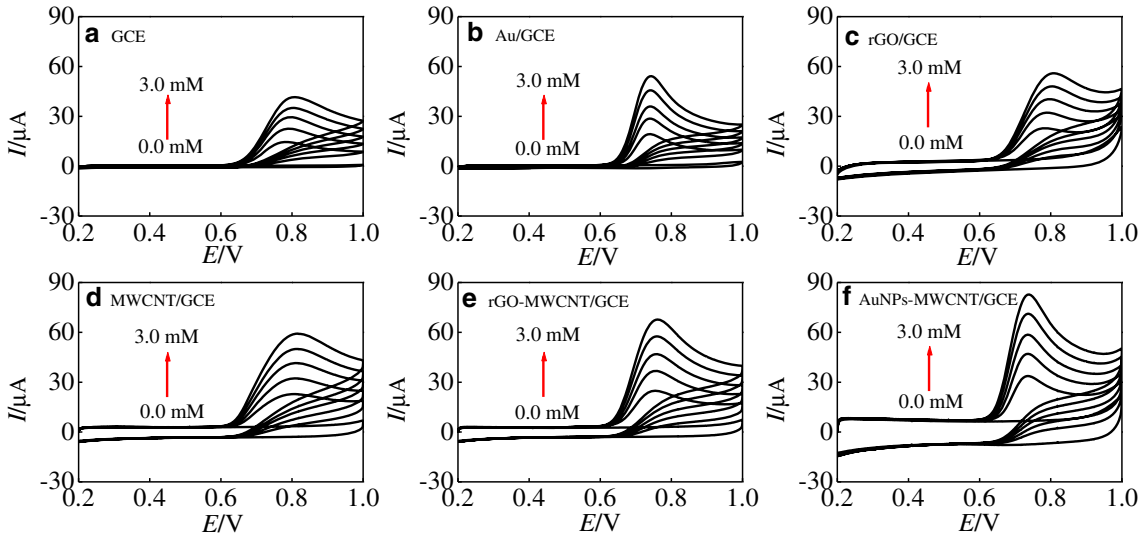

Fig. 3 CV graphs of various electrodes of GCE (**a**), AuNP/GCE (**b**), rGO/GCE (**c**), MWCNTs/GCE (**d**), rGO-MWCNTs/GCE (**e**) and AuNP-rGO-MWCNTs/GCE (**f**) in 0.10 mol·L^{-1} phosphate buffer (pH 5.0) containing different concentration of nitrite (0.0–3.0 mM), potential scan rate, 20 mV·s^{-1}

nitrite is at 0.735 V, and the peak is more sharply. The slope of the linear relationship is 26.03 μA·mM^{-1} (Fig. 3f and Fig. S2, curve f, ESM). By contrast, AuNP-rGO-MWCNTs/GCE exhibits higher electrochemical capability for the electrode process of nitrite as expected.

Cyclic voltammograms (only the oxidation branch is given) of this AuNP-rGO-MWCNTs/GCE in phosphate buffer containing 1.0 mM nitrite with various pH value (2.0–8.0) are shown in fig. S3-A (ESM). As can be seen from this figure, the peak potential (E_p) of nitrite shifts negatively when the pH increase from 2.0 to 4.0. Moreover, when pH is less than 3.0, there is a linear relationship between E_p and pH ($E_{p,a}$ (V) = 0.915–0.053 pH, Fig. S3-B, ESM). This is because of that, under acidic conditions, most nitrite anions have been protonated to form HNO_2 (since the pK_a of HNO_2 is 3.3) [13]. Reports from literatures have also shown that at higher acidity conditions (pH < 3) the peak potential value in nitrite voltammograms is shifted 60 mV·pH^{-1} unit owing to the formation of HNO_2 [32, 33]. However, in the range of pH 4.0–8.0, the peak potential of nitrite almost does not shift with pH (the relationship between E_p and pH is E_p (V) = 0.737–9.87 × 10^{-5} pH, Fig. S3-B, ESM). This may be due to the fact that the electrode process is controlled by kinetic factors rather than thermodynamic factors, indicating that it is a proton independent step when pH is greater than 4 [13]. It is interesting that the pH at the intersection of these two straight lines is 3.36, which is equal to the value of pK_a of nitrite [13].

The peak current (I_p) of nitrite increases at first and then decreases when pH increases from 2.0 to 8.0. The peak current reaches the maximum in pH 4.0–6.0 (Fig. S3-C, ESM). It is noted that, when pH exceeds 7.0, the gold on the electrode surface can form the oxide layers at the high potential, which generates the background current. So the value of the peak current after pH 7.0 is measured by deducting the background current (see Fig. S4, ESM). In low pH solution, NO_2^- will protonate to form HNO_2, which is not conducive to electrode reaction, so the peak current is down [13]. However, under alkaline conditions, AuNP on the surface of the electrode will be oxidized to form an oxide layer, which will inhibit the electrode reaction of nitrite and affect the stability of the electrode [13, 34]. In this study, phosphate buffer with pH 5.0 is selected as the base solution for the determination of nitrite.

Figure S5-A (ESM) gives the CV graphs of the modified GCE recorded in phosphate buffer (pH 5.0) containing 1.0 mM nitrite at various potential scan rates (v). As it can be seen, in the range of 10–150 mV·s^{-1}, the peak currents (I_p) of nitrite increase linearly with the square root of v. The linear regression plot is I_p (μA) = 3.237 + 172.4 $v^{1/2}$ (V·s^{-1})$^{1/2}$, r = 0.998 9 (Fig. S5-B, ESM). The results show that the electrode process is controlled by the diffusion rate of nitrite. Accordingly, the peak potential (E_p) increases linearly with the logarithm of scan rate (log v) in 20–100 mV·s^{-1}, (E_p (V) = 0.817 + 0.0510 log v (V·s^{-1}), see Fig. S5-C, ESM). Based on the Tafel equation, the electron transfer number of electrode reaction in this scan rate range is 2 (assuming α = 0.58), indicating the electrode reaction of nitrite at low scan rate is a two electrons process. The electro-oxidation process of nitrite on common solid electrode has been fully studied. It is generally believed that the electrode process of nitrite in neutral and weakly acidic media consists the following two steps [13, 33, 34]:

$$NO_2^- = NO_2 + e^- \quad (1)$$

$$2NO_2 + H_2O = NO_2^- + NO_3^- + 2H^+ \quad (2)$$

Firstly, nitrite ions are oxidized to NO_2 on the electrode surface, and then NO_2 undergoes second-order homogeneous disproportionation reaction to generate nitrate ions. When the

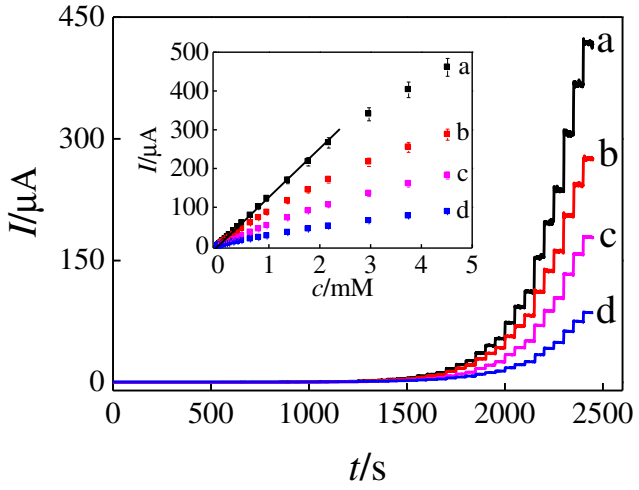

Fig. 4 Amperometric response of different concentration of nitrite on AuNP-rGO-MWCNTs/GCE (**a**), rGO-MWCNTs/GCE (**b**), MWCNTs/GCE (**c**) and rGO/GCE (d) at 0.80 V in 0.10 mol·L^{-1} phosphate buffer (pH 5.0), concentration of nitrite, 0.050–1000 μM (see Fig. S7 in ESM for detail information), insert graph, the calibration plots of the corresponding electrode, rotating speed: 200 rpm

potential scan rate is slow, the whole electrode process is controlled by the total reaction of Eqs.1 and 2, which can be described as Eq.3 [13, 33, 34]:

$$NO_2^- + H_2O = NO_3^- + 2H^+ + 2e^- \quad (3)$$

However, in the range of 100–350 mV·s^{-1}, the linear regression equation between E_p and log v changes to: E_p (V) = 0.870 + 0.102 log v (V·s^{-1}) (Fig. S5-C, ESM). Based on the Tafel equation, the electron transfer number in this scan rate range is 1 (assuming $\alpha = 0.58$). This may be due to the fact that when the scanning rate is high, the homogeneous disproportionation reaction of NO_2 in solution is too late to proceed, and the electrode reaction is mainly controlled by Eq.1, thus apparently showing a one-electron reaction.

Amperometric determination of nitrite

In this work, the more sensitive amperometry is used for the quantitative determination of nitrite. In order to further enhance the analytical performance of the sensor, the working potential is firstly optimized. Fig. S6 (ESM) are the amperometric responses of this AuNP-rGO-MWCNTs/GCE in the potential range from 0.50 to 0.90 V in 0.10 mol·L^{-1} phosphate buffer (pH 5.0) with ten successive 20.0 μM nitrite additions. It is obvious, when the detection potential is 0.8 V, the current has reached the limit current (insert graph of Fig. S6, ESM). So, 0.8 V is selected as the working potential for detection of nitrite.

Under the optimized conditions, the amperometric response of different modified electrodes of AuNP-rGO-MWCNTs/GCE (curve a), rGO-MWCNTs/GCE (curve b), MWCNTs/GCE (curve c) and rGO/GCE (curve d) for nitrite are diplayed in Fig. 4. In this figure, the concentration of nitrite increases from 0.050 μM to 1.0 mM (each concentration is added three times in parallel, see Fig. S7 in ESM for more information). As is obvious to see, the AuNP-rGO-MWCNT/GCE has a greater current response for nitrite than that of other modified electrodes. The linear range of nitrite on AuNP-rGO-MWCNT/GCE is from 5.0×10^{-8} to 2.2×10^{-3} mol·L^{-1} (insert graph of Fig. 4). The calibration plot is I (μA) = − 0.0012 + 126.1 c (mM), r = 0.999 7, with the detection limit of 14 nM (at an SNR of 3). The electrochemical sensitivity is 1201 μA·mM^{-1}·cm^{-2} (the electrode area is measured from CV graph using $K_3Fe(CN)_6$ as electrochemical probe, which is 0.105 cm^2), respectively. The response time is less than 5 s. Table 1 compares the analytical performance of the present sensor with other reported nitrite electrochemical sensors

Table 1 Comparison of analytical performance of the new GCE with other gold nanoparticles based nitrite sensors

Electrode modifier	Methods	Linear range (μM)	LOD (μM)	Sensitivity (a. μA·mM^{-1} b. μA·mM^{-1}·cm^{-2})	Ref
AuNPs/CP	Amperometry	1–30, 40–100	0.093	81.3[a]	[2]
AuNPs/CLDH	Amperometry	1–191	0.5	382.2[a]	[3]
GC/Au-MOF-5	CV	5.0–6500	1.0	9.2[a]	[10]
Au-PPy	DPV	0.5–60	NA	226[b]	[11]
Dendrimer/AuNPs-I	Amperometry	10–5000	0.2	44.8[a]	[12]
GNPs/MWCPE	DPV	0.05–250	0.01	640[b]	[13]
CDs/Au nanohybrids/N	Amperometry	0.1–2000	0.06	35.0[a]	[14]
AuNPs-SGr	DPV	12.5–680	0.0032	418[a]	[15]
RGO–C60/AuNPs	Amperometry	0.05–1175	0.013	536[a]	[16]
AuNPs/GO-SH	Amperometry	5.0–200	0.25	846[a]	[17]
		200–1000		288[a]	
Au/f-GE	DPV	0.125–20,376	0.01	35.7[a]	[18]
GO-CNTs-PMA-Au	DPV	2.0–10,000	0.67	483[b]	[19]
AuNPs/rGO HMS	Amperometry	5.0–1000	0.5	44.0[a]	[20]
		1000–2600		32.2[a]	
rGO-Nf@Au	Amperometry	1.0–160	0.5	62.1[a]	[21]
ERGO/AuNPs	DPV	1–6000	0.13	304.8[b]	[22]
AuNPs-rGO-MWCNTs	Amperometry	0.05–2200	0.014	1201[b]	This work

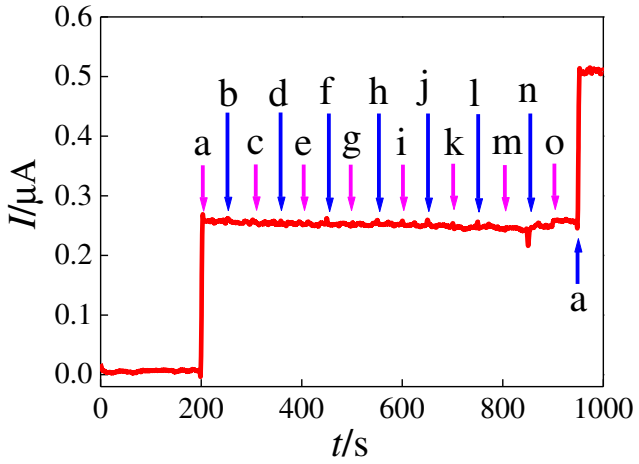

Fig. 5 Amperometric response of 2.0 μM nitrite (**a**) and different concentrations of interfering substances of 1.0 mM KNO_3 (**b**), $NaNO_3$ (**c**), $Ca(NO_3)_2$ (**d**), and $Mg(NO_3)_2$ (**e**), 0.4 mM $Zn(NO_3)_2$ (**f**), $Mn(NO_3)_2$ (**g**), $Ni(NO_3)_2$ (**h**), $Cu(NO_3)_2$ (**i**), $Fe(NO_3)_3$ (**j**), $AgNO_3$ (**k**), Na_2SO_4 (**l**), Na_2CO_3 (**m**), Na_3PO_4 (**n**), and $Fe(SO_4)_2$ (o)

based on AuNP. It can be seen, this AuNP-rGO-MWCNT/GCE shows the outstanding characteristics of wide linear range, low detection limit and high sensitivity [2, 3, 10–22]. This is because of that this AuNP-rGO-MWCNTs nanocomposite has higher electrocatalytic capability for nitrite under the synergistic action of each component in composite.

Selectivity

Figure 5 is a typical amperometric $I-t$ curve recorded with the addition of 2.0 μM nitrite and some possible interfering substances. As it can be seen, the error in current response caused by 500 fold of Ca^{2+}, and Mg^{2+}, 200 fold of Zn^{2+}, Ag^{+}, Mn^{2+}, Ni^{2+}, Cu^{2+}, Fe^{3+}, SO_4^{2-}, CO_3^{2-}, PO_4^{3-}, and Fe^{2+} is less than 5%. Nitrate has no effect on the determination of nitrite. However, in the determination of nitrite by electrooxidation principle, the interference of easily oxidized substances such as Cl^-, Br^-, I^- and SO_3^{2-} in water sample should be noticed. Fig. S8 (ESM) is the amperometric response of 2.0 μM nitrite and different concentration of Cl^- (A), Br^- (B), I^- (C), and SO_3^{2-} (D). As shown in this figure, 200-fold Cl^- can introduces an error of 4.8%. An error of 1-fold Br^-, I^- and SO_3^{2-} is 31%, 77%, and 11%, respectively. Nevertheless, in general, the concentration of the above ions in natural water is very low, and their interference for nitrite can be ignored. It is noticed, chloride ion in water is generally mM grade, and nitrite ion is μM grade. Therefore, the direct determination of nitrite in water samples, chloride ions may interfere. Chloride can precipitate AgCl with $AgNO_3$, so the interference of Cl^- can be eliminated by adding appropriate amount of $AgNO_3$ to water samples. $AgNO_3$ can also precipitate Br^-, I^-, and SO_3^{2-}, which further improving the selectivity. These results show that the resulting sensor has good selectivity in the detection of nitrite in water.

Sample analysis

The practicability and reliability of this AuNP-rGO-MWCNTs/GCE have been evaluated by applying it to analysis of nitrite in the local river water and the spiked samples. Firstly, the original river water has been filtered with filter paper and a 0.45 μm membrane respectively. Then, different concentrations of the spiked samples have been prepared by adding proper amount of $NaNO_2$ to this river water. Subsequently, a proper amount of $AgNO_3$ solution is added to 50.00 mL water sample and the spiked samples (the amount of $AgNO_3$ is determined by Mohr method). After the precipitation, the solution is heated and boiled for 30 min. Finally, these water samples have been filtered with a 0.45 μm membrane. The $I-t$ curve is recorded at 0.80 V in 10 mL supporting electrolyte solution under stirring conditions with the addition of 1.00 mL river water and a certain amount of the spiked samples. The concentration of NO_2^- in these samples has been determined by the standard curve method. The results are shown in Table 2. As is seen in Table 2, the obtained values for recoveries are good and acceptable, which demonstrating that this AuNP-rGO-MWCNTs/GCE can be used for the determination the concentration of nitrite in natural water.

Table 2 Determination results and the recoveries of nitrite in river water ($n = 5$)

Sample	Found by sensor (μM)	RSD (%)	Added (μM)	Total found (μM)	RSD (%)	Recovery (%)
River water	0.121	3.7	0.30	0.386	2.9	88.2
			0.60	0.689	1.3	94.6
			1.00	1.14	1.7	101.7
			3.00	2.83	2.4	90.4
			6.00	5.92	4.3	96.6
			10.0	10.4	3.1	102.7

Stability and reproducibility of the electrode

The working stability of this AuNP-rGO-MWCNTs/GCE is investigated using amperometry by continuous 30 times measurement of 25.0 μM nitrite (Fig. S9-A, ESM). As shown in this figure, the electrode shows a good linear response to nitrite. The linear equation is I (μA) = 0.0038 + 124.8 c (mM), with the correlation coefficient of 0.999 8 (Fig. S9-B, ESM). The results show that the electrode has good working stability. The modified electrode is stored at room temperature for 30 days. Then it is used for determination of 25.0 μM nitrite every day. There is no obvious decrease in current response, meaning a good long-term stability. To evaluate the reproducibility, five modified electrodes have been prepared by the same procedure. Then, they are used for measurement 25.0 μM nitrite solution. The relative standard deviation (RSD) of current response is 4.1%.

Conclusion

A AuNP-rGO-MWCNT nanocomposite has been prepared and characterized. The addition of MWCNTs in composite can improve the dispersibility of rGO and enhance the effective surface area of the material. The AuNP prepared in this system has smaller size, larger loading capacity and higher catalytic activity for the electro-oxidation of nitrite. This multi-component nanocomposite electrochemical sensor exhibits some attractive analytical characteristics including low detection limit, wide dynamic range, high sensitivity, and good stability, which provide a promising platform for determination of nitrite in natural water.

Acknowledgments We would like to thank the support by the Special Research Fund of Education Department of Shaanxi Province, Grant Number: 17JS139, and the Natural Science Fund of Shaanxi Province in China, Grant Number: 2018JM2053.

Compliance with ethical standards The author(s) declare that they have no competing interests.

References

1. Manikandan VS, Adhikari BR, Chen A (2018) Nanomaterials based electrochemical sensors for the safety and quality control of foods and beverages. Analyst 143:4537–4554. https://doi.org/10.1039/C8AN00497H
2. Wan Y, Zheng YF, Yin HY, Song XC (2016) Au nanoparticles modified carbon paper electrode for electrocatalytic oxidation nitrite sensor. New J Chem 40:3635–3641. https://doi.org/10.1039/C5NJ02941D
3. Cui L, Meng XM, Xu MR, Shang K, Ai SY, Liu YP (2011) Electrooxidation nitrite based on copper calcined layered double hydroxide and gold nanoparticles modified glassy carbon electrode. Electrochim Acta 56:9769–9774. https://doi.org/10.1016/j.electacta.2011.08.026
4. Liu Y, Zhou J, Gong J, Wu WP, Bao N, Pan ZQ, Gu HY (2013) The investigation of electrochemical properties for Fe_3O_4@Pt nanocomposites and an enhancement sensing for nitrite. Electrochim Acta 111:876–887. https://doi.org/10.1016/j.electacta.2013.08.077
5. Shen Y, Rao DJ, Bai WS, Sheng QL, Zheng JB (2017) Preparation of high-quality palladium nanocubes heavily deposited on nitrogen-doped graphene nanocomposites and their application for enhanced electrochemical sensing. Talanta 165:304–312. https://doi.org/10.1016/j.talanta.2016.12.067
6. George JM, Antony A, Mathew B (2018) Metal oxide nanoparticles in electrochemical sensing and biosensing: a review. Microchim Acta 185:358. https://doi.org/10.1007/s00604-018-2894-3
7. Annalakshmi M, Balasubramanian P, Chen SM, Chen TW (2019) Amperometric sensing of nitrite at nanomolar concentrations by using carboxylated multi walled carbon nanotubes modified with titanium nitride nanoparticles. Microchim Acta 186:8. https://doi.org/10.1007/s00604-018-3136-4
8. Dai J, Deng DL, Yuan YL, Zhang JH, Deng F, He S (2016) Amperometric nitrite sensor based on a glassy carbon electrode modified with multi-walled carbon nanotubes and poly(toluidine blue). Microchim Acta 183:1553–1561. https://doi.org/10.1007/s00604-016-1773-z
9. Xu JH, Wang YZ, Hu SS (2017) Nanocomposites of graphene and graphene oxides: Synthesis, molecular functionalization and application in electrochemical sensors and biosensors. A review. Microchim Acta 184:1−44. https://doi.org/10.1007/s00604-016-2007-0
10. Yadav DK, Ganesan V, Sonkar PK, Gupta R, Rastogi PK (2016) Electrochemical investigation of gold nanoparticles incorporated zinc based metal-organic framework for selective recognition of nitrite and nitrobenzene. Electrochim Acta 200:276–282. https://doi.org/10.1016/j.electacta.2016.03.092
11. Pineda EG, Rodriguez Presa MJ, Gervasi CA, Bolzan AE (2018) Tubular-structured polypyrrole electrodes decorated with gold nanoparticles for electrochemical sensing. J Electroanal Chem 812:28–36. https://doi.org/10.1016/j.jelechem.2018.01.047
12. Losada J, Garcia Armada MP, García E, Casado CM, Alonso B (2017) Electrochemical preparation of gold nanoparticles on ferrocenyl-dendrimer film modified electrodes and their application for the electrocatalytic oxidation and amperometric detection of nitrite. J Electroanal Chem 788:14–22. https://doi.org/10.1016/j.jelechem.2017.01.066
13. Afkhami A, Soltani-Felehgari F, Madrakian T, Ghaedi H (2014) Surface decoration of multi-walled carbon nanotubes modified carbon paste electrode with gold nanoparticles for electro-oxidation and sensitive determination of nitrite. Biosens Bioelectron 51:379–385. https://doi.org/10.1016/j.bios.2013.07.056
14. Zhuang ZJ, Lin HQ, Zhang X, Qiu F, Yang HY (2016) A glassy carbon electrode modified with carbon dots and gold nanoparticles for enhanced electrocatalytic oxidation and detection of nitrite. Microchim Acta 183:2807–2814. https://doi.org/10.1007/s00604-016-1931-3
15. Bhat SA, Pandit SA, Rather MA, Rather GM, Ingole PP, Rashid N, Bhat MA (2017) Self-assembled AuNPs on Sulphur-doped graphene: a dual and highly efficient electrochemical sensor for nitrite (NO_2^-) and nitric oxide (NO). New J Chem 41:8347–8358. https://doi.org/10.1039/C7NJ01565H
16. Chen S, Thirumalraj B, Chellakannu R, Palanisamy S (2016) Novel electrochemical preparation of gold nanoparticles decorated on a reduced graphene oxide–fullerene composite for the highly sensitive electrochemical detection of nitrite. RSC Adv 6:68798–68805. https://doi.org/10.1039/C6RA10690K
17. Pan F, Chen DD, Zhuang XM, Wu XR, Luan F, Zhang S, Wei JR, Xia S, Li X (2018) Fabrication of gold nanoparticles/L-cysteine functionalized graphene oxide nanocomposites and application for nitrite detection. J Alloys Compd 744:51–56. https://doi.org/10.1016/j.jallcom.2018.02.053

18. Zou CE, Yang BB, Bin D, Wang J, Li SM, Yang P, Wang CQ, Shiraishib Y, Du YK (2017) Electrochemical synthesis of gold nanoparticles decorated flower-like graphene for high sensitivity detection of nitrite. J Colloid Interface Sci 488:135–141. https://doi.org/10.1016/j.jcis.2016.10.088
19. Rao DJ, Sheng QL, Zheng JB (2016) Self-assembly preparation of gold nanoparticle decorated L-pyrenemethylamine functionalized graphene oxide–carbon nanotube composites for highly sensitive detection of nitrite. Anal Methods 8:4926–4933. https://doi.org/10.1039/C6AY01316C
20. Zhang F, Yuan YW, Zheng YQ, Wang H, Liu TH, Hou SF (2017) A glassy carbon electrode modified with gold nanoparticle-encapsulated graphene oxide hollow microspheres for voltammetric sensing of nitrite. Microchim Acta 184:1565–1572. https://doi.org/10.1007/s00604-017-2264-6
21. Yusoff N, Rameshkumar P, Shahid MM, Huang ST, Huang NM (2017) Amperometric detection of nitric oxide using a glassy carbon electrode modified with gold nanoparticles incorporated into a nanohybrid composed of reduced graphene oxide and Nafion. Microchim Acta 184:3291–3299. https://doi.org/10.1007/s00604-017-2344-7
22. Jian JM, Fu LF, Ji JY, Lin LW, Guo XS, Ren TL (2018) Electrochemically, reduced graphene oxide/gold nanoparticles composite modified screen-printed carbon electrode for effective electrocatalytic analysis of nitrite in foods. Sensors Actuators B 262:125–136. https://doi.org/10.1016/j.snb.2018.01.164
23. Woo S, Kim YR, Chung TD, Piao YZ, Kim H (2012) Synthesis of a graphene-carbon nanotube composite and its electrochemical sensing of hydrogen peroxide. Electrochim Acta 59:509–514. https://doi.org/10.1016/j.electacta.2011.11.012
24. Wang F, Wu YJ, Sun XT, Wang LZ, Lu K (2018) Direct electron transfer of hemoglobin at 3D graphene-nitrogen doped carbon nanotubes network modified electrode and electrocatalysis toward nitromethane. J Electroanal Chem 824:83–90. https://doi.org/10.1016/j.jelechem.2018.07.041
25. Zheng ZX, Du YL, Wang ZH, Fen QL, Wang CM (2013) Pt/graphene–CNTs nanocomposite based electrochemical sensors for the determination of endocrine disruptor bisphenol a in thermal printing papers. Analyst 138:693–701. https://doi.org/10.1039/C2AN36569C
26. Jeong H, Nguyen DM, Lee MS, Kim HG, Ko SC, Kwac LK (2018) N-doped graphene-carbon nanotube hybrid networks attaching with gold nanoparticles for glucose non-enzymatic sensor. Mat Sci Eng C 90:38–45. https://doi.org/10.1016/j.msec.2018.04.039
27. Nayak P, Santhosh PN, Ramaprabhu S (2014) Synthesis of Au-MWCNT–graphene hybrid composite for the rapid detection of H_2O_2 and glucose. RSC Adv 4:41670–41677. https://doi.org/10.1039/C4RA05353B
28. Feng QL, Du YL, Zhang C, Zheng ZX, Hu FD, Wang ZH, Wang CM (2013) Synthesis of the multi-walled carbon nanotubes-COOH/graphene/gold nanoparticles nanocomposite for simple determination of bilirubin in human blood serum. Sensors Actuators B 185:337–344. https://doi.org/10.1016/j.snb.2013.05.035
29. Zhao ZT, Sun YJ, Li PW, Zhang WD, Lian K, Hu J, Chen Y (2016) Preparation and characterization of AuNPs/CNTs-ErGO electrochemical sensors for highly sensitive detection of hydrazine. Talanta 158:283–291. https://doi.org/10.1016/j.talanta.2016.05.065
30. Zhao Y, Qin J, Xu H, Gao SM, Jiang TT, Zhang SX, Jin J (2019) Gold nanorods decorated with graphene oxide and multi-walled carbon nanotubes for trace level voltammetric determination of ascorbic acid. Microchim Acta 186:17. https://doi.org/10.1007/s00604-018-3138-2
31. Dong B, Liu GF, Zhou JT, Wang AJ, Wang J, Jin RF, Lv H (2015) Biogenic gold nanoparticles-reduced graphene oxide nanohybrid: synthesis, characterization and application in chemical and biological reduction of nitroaromatics. RSC Adv 5:97798–97806. https://doi.org/10.1039/C5RA19806B
32. Guidelli R (1972) Voltammetric behavior of nitrite ion on platinum in neutral and weakly acidic media. Anal Chem 44:745–755. https://doi.org/10.1021/ac60312a018
33. Rocha JRC, Kosminsky L, Paixao Thiago RLC, Bertotti M (2001) Anodic oxidation of nitrite at a molybdenum oxide layer. Electroanalysis 13:155–160. https://doi.org/10.1002/1521-4109(200102)
34. Piela B, Wrona PK (2002) Oxidation of nitrites on solid electrodes: I. determination of the reaction mechanism on the pure electrode1surface. J Electrochem Soc 149:E55–E63. https://doi.org/10.1149/1.1502691